1 **SMAD4 promotes somatic-germline contact during oocyte growth**

2 Sofia Granados-Aparici[1,3], Qin Yang[1] and Hugh Clarke[1,2,3]

3 1 Research Institute, McGill University Health Centre, 1001 Boul. Décarie, Montréal, QC, Canada H4A 3J1

4 2 Departments of Obstetrics and Gynecology and Biology, Division of Experimental Medicine, McGill

5 University

6 3 Corresponding authors (sograap@gmail.com; hugh.clarke@mcgill.ca)

7

8

9

Abstract

Development of the oocyte requires physical contact with the surrounding granulosa cells of the follicle, which provide it with essential nutrients and regulatory signals. This contact is achieved through specialized filopodia, termed transzonal projections (TZPs), that extend from the granulosa cells to the oocyte surface. Transforming growth factor (TGFβ) family ligands produced by the oocyte increase the number of TZPs, but how they do so is unknown. Using an inducible Cre recombinase strategy together with expression of green fluorescent protein to verify Cre activity in individual granulosa cells, we examined the effect of depleting the canonical TGFβ mediator SMAD4. We observed a 20-50% decrease in the total number of TZPs in SMAD4-depleted granulosa cell-oocyte complexes, and a 50% decrease in the number of newly generated TZPs when the granulosa cells were reaggregated with granulosa cell-free wild-type oocytes. Three-dimensional image analysis revealed that TZPs of SMAD4-depleted cells were also longer than controls and more frequently oriented towards the oocyte. Strikingly, the transmembrane proteins, N-cadherin and Notch2, were reduced by 50% in these cells. SMAD4 may thus modulate a network of cell adhesion proteins that stabilize the attachment of TZPs to the oocyte, thereby amplifying signalling between the two cell types.

Key words

SMAD / oocyte / filopodia / follicle / signalling

31

32 **Introduction**

33 The development of a healthy oocyte within the ovarian follicle requires continuing contact between the
34 germ cell and the somatic granulosa cells that surround it (Clarke, 2018; Doherty *et al*, 2022; El-Hayek &
35 Clarke, 2016; Li & Albertini, 2013; Marchais *et al*, 2022; Richani *et al*, 2021; Robert, 2021; Xie *et al*, 2023).
36 Signals from the granulosa cells initiate the increase in volume of the oocyte when primordial (non-
37 growing) follicles are activated to enter the growth phase (Nagamatsu *et al*, 2019; Saatcioglu *et al*, 2016;
38 Zhang *et al*, 2014). Subsequently, the granulosa cells provide nucleotides, amino acids and pyruvate to
39 the growing oocyte via gap junctions that connect the two cell types (Clarke, 2018; Marchais *et al.*, 2022;
40 Xie *et al.*, 2023). When gap junctional communication between the two cell types is genetically disrupted,
41 oocytes do not develop normally and cannot be fertilized (Carabatsos *et al*, 2000; Gittens & Kidder, 2005;
42 Simon *et al*, 1997; Winterhager & Kidder, 2015). Once the oocyte reaches full-size, it acquires the ability
43 to undergo the final stage of development, termed meiotic maturation, but is prevented from
44 precociously doing so by cyclic GMP that is produced and transferred to it by the granulosa cells, also via
45 gap junctions (Jaffe & Egbert, 2016; Norris *et al*, 2009; Wigglesworth *et al*, 2013; Zhang *et al*, 2010). In
46 vitro, oocytes can develop normally when enclosed by granulosa cells but not when the granulosa cells
47 are removed and provided in co-culture, further emphasizing the crucial importance of physical contact
48 between the two cell types (Eppig, 1979; Herta *et al*, 2021; O'Brien *et al*, 2003).

49 In primordial follicles, a single layer of squamous granulosa cells surrounds the oocyte and contact it via
50 adherens junctions (Jorgensen, 2013; Mora *et al*, 2012). Following activation of growth, a glycoprotein-
51 rich coat termed the zona pellucida becomes established around the oocyte (Litscher & Wassarman, 2020;
52 Wassarman & Litscher, 2018). The zona pellucida steadily thickens as growth continues, reaching a final
53 thickness of about 7 µm in mice and 15 µm in humans. Despite the barrier imposed by the zona pellucida,

54 the granulosa cells and oocyte maintain direct contact by a dense network of thin filopodia-like
55 projections, termed transzonal projections (TZPs), that grow out from the granulosa cells through the zona
56 pellucida (Albertini & Rider, 1994; Baena & Terasaki, 2019; Clarke, 2022; Macaulay *et al*, 2014; Motta *et*
57 *al*, 1994; Zhang *et al*, 2021). The tips of the TZPs establish contact with the oocyte plasma membrane
58 through heterotypic adherens junctions comprising N-cadherin (granulosa cell) and E-cadherin (oocyte)
59 and harbour the gap junctions that link the two cell types (Mora *et al.*, 2012) and likely also through focal
60 adhesions (McGinnis & Kinsey, 2015). New TZPs are generated throughout follicular growth, thereby
61 increasing intercellular molecular trafficking (El-Hayek *et al*, 2018a), and a genetically imposed decrease
62 in the number of TZPs is associated with defects in oocyte gene expression and development (Crozet *et*
63 *al*, 2023). Despite the essential role of TZPs during oocyte development in mammals and the presence of
64 analogous structures in the ovarian follicles of non-mammalian species (Kessel *et al*, 1985; Schroeder,
65 1981), the molecular mechanisms that govern their generation and stability are little understood.

66 The TGFβ signalling pathway regulates the functions and interactions of a wide range of cell types under
67 various physiological and pathological conditions (Derynck & Budi, 2019; Peng *et al*, 2022). Binding of the
68 ligand to a complex of type I and type II receptors located at the cell surface activates signalling within the
69 cell, most commonly through the members of the SMAD family of transcription factors, although SMAD-
70 independent signaling can also occur (Aashaq *et al*, 2022; Derynck & Budi, 2019). Upon phosphorylation
71 of the tetrameric type II and type I receptors and subsequent phosphorylation of receptor-activated SMAD
72 proteins (R-SMADs; SMAD1, 2, 3, 5 and 8), a heterotrimeric complex with SMAD4 is formed which enters
73 the nucleus and regulates gene expression by binding to specific SMAD-binding DNA elements. Although
74 R-SMADs can signal in the absence of SMAD4, evidence indicates that the presence of SMAD4 in the
75 heterotrimer amplifies TGFβ cell signalling by stabilizing the complex and by favouring the binding of other
76 transcriptional co-repressors or co-activators of target genes (Aragón *et al*, 2019; Guglielmi *et al*, 2021).

77 The TGFβ superfamily members, growth-differentiation factor (GDF) 9 and bone morphogenetic protein
78 (BMP) 15 are produced by the oocyte (Dong *et al*, 1996; Yan *et al*, 2001) and genetic, pharmacological and
79 in vitro studies have revealed multiple roles for TGFβ/SMAD signaling during follicular growth and
80 development (Knight & Glister, 2006; Pangas & Rajkovic, 2015; Patton *et al*, 2021). TGFβ signalling via
81 SMAD3 in granulosa cells acts initially in primordial follicles to maintain their quiescence (Granados-
82 Aparici *et al*, 2019; Wang *et al*, 2014) and later, following their activation, becomes excluded from the
83 nucleus in association with rapid granulosa cell growth and proliferation (Hardy *et al*, 2018). Female mice
84 lacking GDF9 rarely generate more than a single layer of granulosa cells (Dong *et al.*, 1996; Elvin *et al*,
85 1999a; Elvin *et al*, 1999b), due to an up-regulation of inhibin expression (Wu *et al*, 2004), and are
86 consequently infertile. Prior to ovulation, SMAD2/3 signalling in the cumulus granulosa cells, which is
87 activated or maintained by homo- and/or heterodimers of GDF9 and BMP15, is necessary to up-regulate
88 the transcription of genes whose products drive expansion of the cumulus cell layer, a pre-requisite for
89 fertilization (Dragovic *et al*, 2007; Hao *et al*, 2022; Mottershead *et al*, 2015; Peng *et al*, 2013; Yu *et al*,
90 2013).

91 A potential role for TGFβ-SMAD signaling in the generation or maintenance of TZPs was suggested first by
92 observations that TZP morphology is abnormal in mice lacking GDF9 (Carabatsos *et al*, 1998) and later by
93 the observation that their number is reduced in follicles grown in vitro following RNAi-mediated depletion
94 of GDF9 in the oocyte (El-Hayek *et al.*, 2018a). To test the role of SMAD4 specifically, we used a Cre-lox
95 strategy to inactivate *Smad4* in granulosa cells. This approach has previously been used to inactivate
96 *Smad4*, with Cre expression driven by the promoter of either *Amhr2* (anti-Mullerian hormone receptor 2),
97 where Cre activity is observed mainly in granulosa cells of growing follicles (Jorgez *et al*, 2004) or *Cyp19*,
98 where activity is detected in antral follicles (Yu *et al.*, 2013). The former is associated with a range of
99 phenotypes, notably including loss of contact between the oocyte and cumulus cells in some pre-
100 ovulatory follicles and premature luteinization of the granulosa cells (Pangas *et al*, 2006). In the latter,

101 changes in granulosa cell gene expression and a failure to undergo cumulus layer expansion were
102 observed (Yu *et al.*, 2013). However, the interactions between the oocyte and granulosa cells were not
103 specifically examined in these studies.

104 Using image analysis tools and three-dimensional reconstructions, we show that depletion of SMAD4 in
105 the granulosa cells decreases the number of TZPs that project from individual granulosa cells in both intact
106 granulosa cell-oocyte complexes (GOCs) and in reaggregated complexes. Morphometric parameters
107 including length and orientation are also altered. The decrease in TZP number in intact GOCs is associated
108 with a reduction in the amount of N-cadherin and Notch2 in the granulosa cells, suggesting that the
109 composition of the granulosa cell surface is perturbed in the absence of SMAD4. SMAD4-depleted
110 granulosa cells are, however, able to support the generation of new TZPs as assayed using a
111 reaggregation assay. We propose that SMAD4, through its activity to increase expression of target genes,
112 stabilizes TZPs by promoting their adhesion to the oocyte surface, thereby helping to increase the number
113 of TZPs and communication between the growing oocyte and its follicular microenvironment.

114

115 **Results**

116 We began by verifying the expression of SMAD4 during folliculogenesis. As shown in Fig. 1A and consistent
117 with prior reports, SMAD4 was detectable in primordial and growing follicles as well as in the granulosa
118 cells collected from pre-antral follicles. SMAD2 and SMAD3 were also present, with SMAD2 being the
119 major species detected in oocytes. Two strategies were tested to deplete SMAD4 from the granulosa cells
120 of growing follicles. First, mice were generated carrying two floxed *Smad4* alleles and a transgene
121 encoding Cre recombinase under the control of the *Amhr2* promoter (Fig. 1B). These mice also carried a
122 transgene (*mTmG*, see Methods) constructed such that Tomato fluorescent protein is expressed in the

123 absence of Cre activity, whereas Cre-mediated recombination switches expression to green fluorescent
124 protein (GFP), thus allowing us to identify cells where Cre had been active. Upon immunostaining of
125 ovarian sections or whole-mount intact follicles, only a small number of cells expressed GFP (Fig. 1C, left).
126 Consistent with this observation, less than 10% of FACS-sorted granulosa cells were GFP-positive (Fig. 1C,
127 right). Thus, in our system, *Amhr2-Cre* did not mediate efficient recombination of floxed DNA in granulosa
128 cells.

129 We therefore turned to mice that expressed Cre under the control of a tamoxifen-inducible form of the
130 estrogen receptor (ER) gene promoter (*ER-Cre*). Because ER is expressed in pituitary gonadotropes and
131 SMAD4 regulates the transcription of the *Fshb* gene encoding the β-subunit of follicle-stimulating
132 hormone (Li *et al*, 2018), this model could not be used in vivo. Granulosa cell-oocyte complexes (GOCs)
133 from mid-growth stage follicles (diameter 100-120 µm) were therefore isolated, exposed to tamoxifen for
134 one day and then incubated in tamoxifen-free medium for another five days. Under these conditions, a
135 substantial fraction of the granulosa cells underwent Cre-mediated recombination, as indicated by the
136 expression of GFP in immunostained GOCs and by FACS analysis (Fig. 1E). This in vitro system was used
137 for the experiments described here.

138 To examine the efficiency of Cre-mediated *Smad4* recombination, the mRNA level was assessed in intact
139 GOCs using the RNAscope technique and in purified granulosa cells using qRT-PCR. Following tamoxifen
140 treatment and culture, there was an approximately 60% reduction in the number of foci in the granulosa
141 cells from 5.78 +/- 0.36 (mean, s.e.m., n=21) in *ER-Cre*$^{-}$; *Smad4*$^{fl/fl}$ mice to 2.16 +/- 0.26 (n=26) in *ER-Cre*$^{+}$;
142 *Smad4*$^{fl/fl}$ mice (p<0.0001), and a 70% reduction in the amount of PCR product from granulosa cells (n=5,
143 p=0.0001) (Fig. 1F). Immunoblotting of granulosa cells revealed a corresponding 70% reduction in SMAD4
144 protein in the granulosa cells of *ER-Cre*$^{+}$; *Smad4*$^{fl/fl}$ mice compared to *ER-Cre*$^{-}$; *Smad4*$^{fl/fl}$ controls (n=11,

145 $p<0.0001$) (Fig. 1G). Thus, the in vitro ER-Cre strategy substantially reduced although did not eliminate
146 SMAD4 from the granulosa cells.

147 To examine the effect of SMAD4 depletion on the TZPs, GOCs were isolated and cultured as above, fixed
148 and stained using anti-GFP to label cells where Cre had been active and phalloidin to label the TZPs, and
149 imaged them using confocal microscopy. First, the TZPs were analyzed as a population. Because TZPs arise
150 from both the innermost and more distal granulosa cell layers (Baena & Terasaki, 2019), it was not possible
151 to reliably determine how many granulosa cells contributed the GFP-positive TZPs in a GOC. The total
152 number of phalloidin-stained TZPs – irrespective of whether they were GFP-positive – that projected to
153 the oocyte in equatorial optical sections of GOCs from control (*Smad4*$^{wt/wt}$) and experimental (*Smad4*$^{fl/fl}$)
154 mice were therefore counted (Fig. 2A, B). TZP-number was normalized to the diameter of the
155 corresponding oocyte, although the mean oocyte diameter did not differ between the groups (Fig. 2B),
156 We observed a 20.4 +/- 0.05% reduction in the number of TZPs in the GOCs from the *Smad4*$^{fl/fl}$ mice (n=63
157 [control], 59 [experimental], $p=0.002$).

158 A limitation of quantifying TZPs in intact GOCs is that the granulosa cells, depending on their number and
159 spatial distribution, can variably impair their resolution and discrimination even using confocal
160 microscopy. Therefore, the number of TZPs was also counted after mechanically removing the granulosa
161 cells from the GOCs. This analysis revealed a striking 51.1 +/- 0.04% reduction in the normalized number
162 of TZPs in the GOCs from the *Smad4*$^{fl/fl}$ mice (n=44 [control], 47 [experimental], $p<0.0001$) (Fig. 2C, D). As
163 observed using intact GOCs, the mean oocyte diameter did not differ (Fig. 2D). To verify the difference in
164 TZP-number, we also compared *ER-Cre*$^{+}$; *Smad4*$^{fl/fl}$ to a different control genotype, *ER-Cre*$^{-}$; *Smad4*$^{fl/fl}$ mice.
165 A quantitatively similar 43.6 +/- 0.04% decrease in TZPs within the *ER-Cre*$^{+}$ population (n=164 [control],
166 172 [experimental], $p<0.0001$) (Fig. 2D) was observed following tamoxifen treatment and culture.

167 Together, these results indicate that depletion of SMAD4 in the granulosa cells is associated with a
168 decrease in the number of TZPs.

169 TZPs provide the physical platform that enables essential gap junctional communication between the
170 granulosa cells and the oocyte. To test whether the reduction in TZP number in SMAD4-depleted
171 granulosa cells impaired this communication, we used a fluorescence recovery after photobleaching
172 (FRAP) assay. Control and experimental GOCs were treated with tamoxifen and incubated as above. After
173 five days, they were exposed to calcein-AM, a fluorescent dye that can pass through gap junctions. The
174 fluorescence in the oocyte of each GOC was bleached using the laser of a confocal microscope and its
175 recovery was then recorded. As shown in Fig. 2E, which plots the fluorescence in the oocyte as a function
176 of time after photobleaching and at the end of the recording period normalized to the initial fluorescence,
177 we observed no difference between groups in the rate of transfer of fluorescence from the granulosa cells
178 to the oocyte. Thus, despite the decreased number of TZPs, depletion of SMAD4 did not detectably impair
179 gap junctional communication between the granulosa cells and the oocyte.

180 As TZPs project not only from the cells immediately adjacent to the zona pellucida but also from those in
181 more distal layers, it was possible that the reduced number of TZPs in *ER-Cre*$^{+}$; *Smad4*$^{fl/fl}$ complexes
182 reflected an impaired ability of the granulosa cells to proliferate. *ER-Cre*$^{+}$*; Smad4*$^{+/+}$ and *ER-Cre*$^{+}$*; Smad4*$^{fl/fl}$
183 GOCs were incubated for 5 hr in the presence of the thymidine analogue, EdU, added five days after the
184 tamoxifen exposure. No difference between the groups in the fraction of EdU-positive cells was observed
185 (Fig. 2F), however, implying that the reduced number of TZPs was not due to impaired proliferation of the
186 granulosa cells.

187 We then focused our analysis on individual granulosa cells. GOCs where individual GFP-positive cells could
188 be readily identified and the TZPs were easily attributable to a particular cell (Fig. 3A) were selected, serial
189 optical sections were obtained using confocal microscopy, and 3-dimensional images were reconstructed

190 using Imaris software. Fig. 3B shows one such reconstruction, where GFP-positive granulosa cells are
191 pseudo-coloured in green. We observed a 25% decrease in the mean volume of *Smad4*$^{fl/fl}$ granulosa cells
192 compared to wild-type cells (323.2 +/- 11.2 vs 242.6 +/- 10.0; n=293, 322; p<0.0001), but no difference
193 between genotypes in the sphericity of the cells (Fig. 3C). The TZPs in a subset of the GFP-positive
194 granulosa cells were then analyzed (Fig. 3D). In this subset, there was a 15% difference in mean cell volume
195 (392.2 +/- 20.8 vs 334.0 +/- 21.2; n=55, 63) which did not reach statistical significance (p=0.054). However,
196 whereas wild-type cells harbored a mean of 15.8 +/- 0.87 (n=55) TZPs per cell, this number was reduced
197 by 35% in *Smad4*$^{fl/fl}$ cells to 10.5 +/- 0.71 (n=65, p<0.0001). As compared to those of wild-type cells, the
198 TZPs of the *Smad4*$^{fl/fl}$ cells were about 10% longer (4.64 +/- 0.08 µm vs 5.19 +/- 0.09 µm; n=893, 720;
199 p<0.0001) and very slightly narrower (0.40 +/- 0.003 µm vs 0.38 +/- 0.003 µm; n=870, 719; p<0.0001)(Fig.
200 3E). We did not detect other differences between the genotypes in TZP morphology. These results
201 obtained using reconstructed 3-dimensional images of GFP-positive cells establish that the number of
202 TZPs is reduced in individual SMAD4-depleted granulosa cells.

203 A limitation of analyzing TZPs in GFP-positive cells within GOCs is that that this strategy cannot distinguish
204 TZPs that were generated in a low-SMAD4 environment (i.e., after the Cre recombinase was expressed)
205 from those generated earlier in a normal-SMAD4 environment. To ensure that we examined only TZPs
206 that were generated after Cre had been expressed, we used our previously published reaggregation assay
207 (El-Hayek *et al.*, 2018a) (Fig. 4A). GOCs obtained from mid-growth stage follicles of *ER-Cre; mTmG* mice
208 carrying the appropriate *Smad4* alleles were exposed to tamoxifen for one day and then incubated for an
209 additional four days. The granulosa cells were then separated from the oocyte and combined with an
210 oocyte that did not carry the *mTmG* gene. These reaggregated GOCs were incubated for an additional 6
211 days, then fixed and stained using anti-GFP (Fig. 4B).

212 When the entire population of granulosa cells in the reaggregated GOCs was analyzed, there was a ~30%
213 reduction in mean volume in the *Smad4*$^{fl/fl}$ cells as compared to *Smad4*$^{+/+}$ cells (394.5 +/- 18.8 vs 279.8 +/-
214 16.6; n=185, 159; p<0.0001) and no difference in cell sphericity (Fig. 4C), as observed using intact GOCs.
215 There was no difference between genotypes, however, in mean volume among the cells whose TZPs were
216 characterized (Fig. 4D). Within this group, the mean number of TZPs per cell was reduced by ~50%, from
217 14.2 +/- 2.0 (n=16) in the *Smad4*$^{+/+}$ cells to 6.84 +/- 1.1 (n=25) in the *Smad4*$^{fl/fl}$ cells (Fig. 4D, p=0.001). A
218 ~20% increase in the mean length of the TZPs of *Smad4*$^{fl/fl}$ cells (3.71 +/- 0.17 vs 4.40 +/- 0.28; n=174, 154;
219 *p*=0.03) was also detected, as in intact GOCs, but no difference in the mean width (Fig. 4E).

220 The increased mean length of the TZPs of *Smad4*$^{fl/fl}$ cells compared to *Smad4*$^{+/+}$ cells prompted us to
221 analyze the trajectory of individual TZPs. We traced their path from their point of origin to their tip, then
222 measured the distance between the point of origin and the oocyte and subtracted from this the distance
223 between the tip and the oocyte. A large positive difference indicates that the tip of the TZP is relatively
224 close to the oocyte; conversely, a small positive or a negative difference indicates that that tip is relatively
225 far from the oocyte (Fig. 4F). This analysis revealed that the mean difference was 50% greater in the
226 *Smad4*$^{fl/fl}$ cells compared to *Smad4*$^{+/+}$ cells (1.61 +/- 0.16 vs 2.40 +/- 0.21; n=174, 157; *p*=0.003) (Fig. 4G).
227 This indicates that the tips of the TZPs of the *Smad4*$^{fl/fl}$ cells were, on average, closer to the oocyte than
228 those of the *Smad4*$^{+/+}$ cells. We also found that the proportion of TZPs that were oriented away from the
229 oocyte trended towards being greater in the *Smad4*$^{+/+}$ cells, although the difference did not reach
230 statistical significance (Fig. 4G). Taken together, the trajectory analyses provide additional evidence that
231 the TZPs of *Smad4*$^{fl/fl}$ cells differ from those of *Smad4*$^{+/+}$ cells.

232 The observation that TZP-number was modestly reduced when intact GOCs were analyzed, yet markedly
233 reduced when oocytes from which the granulosa cells had been stripped were analyzed, suggested that
234 the attachment between the TZPs and oocyte might be weakened when SMAD4 was depleted. To

235 evaluate this, the amount of N-cadherin, which is the principal cell adhesion molecule that has been
236 identified in granulosa cells, was compared between *Smad4*$^{+/+}$ and *Smad4*$^{fl/fl}$ granulosa cells. Consistent
237 with the previous results (see Fig. 1E), SMAD4 was reduced by 73.5 +/- 0.05% in the *Smad4*$^{fl/fl}$ granulosa
238 cells (Fig. 5A, n=6, p<0.0001). Strikingly, N-cadherin was reduced by 52.7 +/- 0.04 % (n = 6, p=0.0004) in
239 the *Smad4*$^{fl/fl}$ granulosa cells (Fig. 5A). Moreover, Notch2, a transmembrane receptor expressed in
240 granulosa cells that associates with membrane-bound Jagged1 expressed on the oocyte, was reduced by
241 52.6 +/- 0.05% (n=5; p=0.0003) in these cells (Fig. 5B). In contrast to the protein, however, there was no
242 detectable reduction in the amount of encoding mRNA in either case as assayed using qRT-PCR, although
243 *Smad4* was reduced in the same samples (Fig. 5C). Thus, a reduction in SMAD4 in granulosa cells is
244 associated with a reduction in certain transmembrane proteins, including those responsible for cell
245 adhesion.

246 As we previously reported that depletion of GDF9, which is secreted by the oocyte and signals in the
247 granulosa cells through SMAD4, was associated with a reduction in mRNAs encoding structural
248 components of TZPs – *Myo10*, *Fscn1*, and *Daam1* (El-Hayek *et al.*, 2018a), we measured the quantity of
249 these mRNAs using qRT-PCR. We found that they were not depleted in the *Smad4*$^{fl/fl}$ granulosa cells
250 compared to the *Smad4*$^{+/+}$ cells (Fig. 5D). This implies either that the SMAD4 which remained was
251 sufficient to induce expression of these genes or the GDF9 regulates their expression through a SMAD4-
252 independent pathway.

253

254 **Discussion**

255 We have examined the role of SMAD4 establishing the TZPs that connect the granulosa cells to the oocyte.
256 Using a tamoxifen-inducible Cre recombinase strategy, we were able to reduce SMAD4 in the granulosa

257 cells to about 30% of its wild-type level. This reduction was associated with a decrease ranging from 20-
258 50% in the number of TZPs in the granulosa cells assessed as a population (i) in intact GOCs and (ii) after
259 removal of the granulosa cell bodies to increase optical resolution, and as individual cells (iii) in intact
260 GOCs and (iv) in reconstructed complexes. Previous studies where SMAD4 was depleted from granulosa
261 cells described a loose or loss association of the cumulus cells with the oocyte in some follicles (Pangas *et*
262 *al.*, 2006; Yu *et al.*, 2013), which is consistent with the idea that that fewer TZPs were available to anchor
263 the cumulus cells to the oocyte. Together these observations suggest that SMAD4 regulates the size of
264 the population of TZPs in growing follicles.

265 The population of TZPs presumably reflects the net result of the generation of new TZPs and the retraction
266 of existing TZPs, as is the case for filopodia (Gallop, 2020; Heckman & Plummer, 2013; Mattila &
267 Lappalainen, 2008). SMAD4 could thus promote either or both processes. The observation that GFP-
268 expressing granulosa cells in reaggregated complexes generated new TZPs implies that SMAD4 is not
269 required for this process, although it does not rule out a role in increasing the rate of generation. A clue
270 to the function of SMAD4 may lie in the observation that the decrease in the number of TZPs in SMAD4-
271 depleted cells was quantitatively greater when the granulosa cell bodies were removed prior to analysis.
272 This suggests that the process of removing the cell bodies also removed the TZPs more easily in the
273 SMAD4-depleted cells than in wild-type cells. In this context, it is intriguing that N-cadherin, which is
274 thought to stabilize attachment of the TZP tips to the oocyte surface, was depleted in the mutant cells.
275 We propose that, by increasing the quantity of N-cadherin in the granulosa cells, SMAD4 increases the
276 strength of adhesion of the TZPs to the oocyte surface (Fig. 6). This in turn would decrease the probability
277 of retraction, thereby increasing the steady-state number of TZPs.

278 This model is consistent with the observation that the non-attached (free-ended) TZPs of SMAD4-depleted
279 cells were on average longer and closer to the oocyte than those of wild-type cells. Specifically, if the

280 ability of the TZPs to establish a stable contact with the oocyte were impaired in SMAD4-depleted cells, a
281 relatively large proportion might continue to 'search' for an attachment and to lengthen during the
282 searching process. Mechanistically, some reports have linked SMAD4 to transcription of the *Cdh2*, which
283 encodes N-cadherin (Kang *et al*, 2014; Yang *et al*, 2015), but we did not detect a difference in mRNA
284 quantity between normal and SMAD4-depleted granulosa cells. In view of the reduced quantity in the
285 latter of Notch2, also a membrane-associated protein, it may be speculated that SMAD4 might act more
286 broadly to regulate the expression of genes whose products maintain the normal configuration of the
287 granulosa cell plasma membrane. Regardless of the mechanism, it is noteworthy that the number of TZPs
288 that project from an individual granulosa cells – about 15 in this study and about 40 in a previous study
289 where more advanced (antral) follicles were examined (Baena & Terasaki, 2019) – considerably exceeds
290 the number of filopodia that are present on individual blastomeres of mouse embryos (5-6) (Fierro-
291 Gonzalez *et al*, 2013) or on chick embryonic cells (~4) (Sagar *et al*, 2015). SMAD4 may therefore act in
292 granulosa cells to amplify an innate ability to generate filopodia, which become TZPs and increase the
293 efficiency of communication between the growing germ cell and its somatic microenvironment.

294

295 **Methods**

296 ***Mouse strains***

297 All experiments were performed in compliance with the regulations and policies of the Canadian Council
298 on Animal Care and were approved by the Animal Care Committee of the Research Institute of the McGill
299 University Health Centre (RI-MUHC, protocol 7783). CD-1 mice were obtained from Charles River (St-
300 Constant, QC). The following transgenic strains were obtained from commercial suppliers: B6.129-
301 *Gt(ROSA)26Sor*$^{tm1(cre/ERT2)Tyj}$/J (hereafter *ER-Cre*) carrying a tamoxifen-inducible sequence encoding Cre

302 recombinase under the control of the promoter of the estrogen receptor 2 gene (Jackson Laboratories,
303 Bar Harbor, ME, strain 008463); B6.129(Cg)-*Gt(ROSA)26Sor*$^{tm4(ACTB\text{-}tdTomato,\text{-}EGFP)Luo}$/J (Jackson, strain 007676;
304 hereafter *mTmG*) carrying sequences encoding a membrane-targeted tdTomato and membrane-targeted
305 EGFP; Cre-mediated recombination of *loxP* sites switches expression from RFP to EGFP. *Smad4*$^{tm2.1Cxd}$/J
306 (hereafter *Smad4*^{fl}) carrying *loxP* sites flanking exon 8 (Jackson, strain 017462) was kindly supplied by Dr.
307 Daniel Bernard (McGill University). *Amhr2*$^{tm3(cre)Bhr}$ (hereafter *Amhr2-Cre*) carrying a sequence encoding
308 Cre recombinase under the control of the promoter of the Anti-Mullerian hormone receptor 2 gene was
309 kindly supplied by Dr. Makoto Nagano (McGill University).

310 To generate *Amhr2-Cre*$^{+}$*; Smad4*$^{fl/fl}$ females carrying an *mTmG* allele, *Smad4*$^{fl/wt}$; *mTmG*$^{+/+}$ females were
311 crossed with *Amhr2-Cre*$^{+}$*; Smad4*$^{fl/wt}$ males. To generate *ER-Cre*$^{+}$*; Smad4*$^{fl/fl}$ females carrying an *mTmG*
312 allele, *Smad4*$^{fl/wt}$; *mTmG*$^{+/+}$ females were crossed with *ER-Cre*$^{+}$*; Smad4*$^{fl/wt}$ males. *ER-Cre*$^{-}$*; mTmG*$^{+}$*;*
313 *Smad4*$^{fl/fl}$ females and *ER-Cre*$^{+}$*; mTmG*$^{+}$*; Smad4*$^{wt/wt}$ females served as controls. Genotyping of the offspring
314 was done using the EZ Tissue/Tail DNA Isolation Plus PCR kit (EZ Bioresearch). After DNA extraction from
315 tail snips, PCR was used to detect wild type, floxed and recombined *Smad4* and the presence of *ER-Cre*
316 and *Amhr2-Cre* alleles. Primer sequences are given in Supplemental Table 1.

317 **Tissue embedding and immunohistochemistry**

318 Sections of paraffin-embedded ovaries were deparaffinized using xylene, rehydrated in a decreasing
319 ethanol series (100, 90, 70%) for 3 min each, and then placed in Milli-Q water for 5 min. Slides were heated
320 intermittently in a microwave during 20 min in 0.1 M citrate buffer solution at pH 6.0, washed in PBS for
321 10 min, and blocked with CAS universal blocking solution (Thermo Fisher, 008120) for 30 min at room
322 temperature to reduce nonspecific binding. After overnight incubation with primary antibody, slides were
323 washed three times in PBS at room temperature and then incubated for 1 h at room temperature with
324 secondary antibody with DAPI. Slides were washed twice in PBS for 5 min and mounted on a drop of

325 VECTASHIELD solution (Vector Laboratories, H-1200-10). Images were acquired using a Zeiss LSM 880
326 confocal microscope.

327 **Collection, culture and tamoxifen treatment of granulosa cell-oocyte complexes (GOCs)**

328 GOCs were obtained as previously described (El-Hayek *et al*, 2018b; O'Brien *et al.*, 2003). Briefly, ovaries
329 of 10- to 12-day-old mice were dissected from the ovarian bursa. Follicles were mechanically isolated by
330 carefully tearing the ovaries apart and using fine needles to separate the follicles from each other in
331 HEPES-buffered minimal essential medium (MEM, pH 7.2, Life Technologies, Burlington, ON) (MEM-H). A
332 Pipetman P1000 was used to carefully pick up and transfer the individual follicles to dishes containing
333 fresh medium. GOCs were obtained by incubating follicles in the presence of collagenase (10 µg/ml;
334 Cedarlane, Burlington, ON) and DNase I (10 µg/ml; Sigma) for 5 min at 37°C in air. GOCs were collected
335 and briefly washed in $NaHCO_3$-buffered MEM (MEM-C) and cultured in 4-well plates containing 500 µl of
336 MEM-C supplemented with ITS (10 µg/mL insulin, 5.5 µg/mL transferrin and 5 ng/mL selenium; Sigma),
337 FSH (10 mIU/ml; EMD Serono, Mississauga, ON), and estradiol (10 nM, Sigma, E2758) in an atmosphere
338 of 5% CO_2 in air. To induce Cre-mediated recombination of the *Smad4* allele, GOCs were incubated with
339 4-hydroxytamoxifen (1 µg/ml, Sigma, T176) in the above medium for 24 hours. They were then transferred
340 to medium without tamoxifen.

341 **Immunoblotting**

342 Cell samples were lysed in 10 µl of Laemmli buffer. After denaturation at 95◦C for 10 min, proteins were
343 separated using 4–15% precast polyacrylamide gels (BioRad, 4568085) and transferred onto a
344 polyvinylidene fluoride membrane (Amersham, Oakville, ON, Canada) under constant voltage. The
345 membrane was subsequently blocked using 5% BSA, in 0.1% Tween-PBS. The membrane was washed
346 three times in Tween-PBS and incubated with primary antibody overnight at 4◦C. After washing for 45

347 min, the membrane was incubated in secondary antibody conjugated to horseradish peroxidase
348 (Promega) at a dilution of 1:5000 for 1h at room temperature. After washing for 30 min, bound antibody
349 was revealed using ECL+ (Amersham). Antibodies used are shown in Supplemental Table 1.

350 **RNA purification and quantitative real-time PCR**

351 RNA was extracted using a Picopure RNA isolation kit (Life Technologies) following the manufacturer's
352 instructions and eluted in 10 µL of the provided elution buffer, as described (El-Hayek *et al*, 2018a). Briefly,
353 SuperScript II Reverse Transcription kit (Life Technologies) was used to generate cDNA. PCR amplification
354 was performed using a Corbett Rotorgene 6000 (Montreal Biotech, Montreal, QC). Each reaction
355 contained 4 µL of EvaGreen Mix (Montreal Biotech), 13 µL of UltraPure DNase/RNase-free distilled water
356 (Life Technologies), 1 µL of 10 mM primers and 2 µL of cDNA (diluted 1:20 from original stock). Primers
357 were designed using Primer-BLAST (National Institutes of Health) and obtained from Sigma. For each
358 primer pair, a standard curve was generated using serial dilutions of cDNA prepared from ovarian RNA
359 and used to determine the efficiency of amplification. Melt-curve analysis and electrophoresis of
360 amplified products confirmed that only a single product of the expected size was generated. Data was
361 analyzed using software provided by the manufacturer. Relative quantities of amplified product were
362 calculated according to 2-ΔΔCT method, using *Rpl19* for normalization. Primers are shown in
363 Supplemental Table 1.

364 **Immunofluorescence**

365 GOCs and denuded oocytes were fixed for 15 min in freshly prepared 2% (w/v) para-formaldehyde (Fisher
366 Scientific 04042) in PBS (pH 7.2) containing 0.1% Triton X-100 (ACROS 9002-93-1) (PBST), then washed in
367 PBST. The specimens were incubated overnight in primary antibody in PBST at 4 °C with gentle agitation,
368 washed twice in PBST, then incubated for 1 h at room temperature in the secondary antibody as well as

369 phalloidin and DAPI in PBST, then washed in PBST. GOCs or denuded oocytes were placed in a 2 µl drop
370 of PBS containing 0.3% polyvinylpyrrolidone (Sigma, PVP360) on a glass bottom dish covered with mineral
371 oil. Images were acquired using a Zeiss LSM880 confocal microscope. Images were obtained as 16-bit RGB
372 stack files. GOCs were imaged with a Plan Apo 63x/1.4 oil immersion objective and the following lasers
373 and filters (in parentheses): 488 nm (491–553 nm), 561 nm (571–642) and 405 nm (410–484). Laser
374 strength ranged between 1.5 and 2% and digital gain was adjusted until the first saturated pixels were
375 observed for each channel.

376 **EdU incorporation and detection**

377 EdU (5-ethynyl-2'-deoxyuridine) detection was performed on GOCs according to the Click-iT EdU Alexa
378 Fluor 488 Imaging Kit manufacturer's instructions (Molecular Probes, C10337). Briefly, cells were
379 incubated in MEM containing 100 µM EdU for 5 hrs to allow for incorporation into newly synthesized DNA,
380 then fixed, permeabilized, and incubated in Click-iT cocktail reaction for 30 minutes. EdU labeling was
381 visualized by confocal microscopy and quantified with ImageJ (NIH).

382 **In situ hybridization**

383 GOCs were fixed in freshly prepared 2% paraformaldehyde in phosphate-buffered saline (PBS, pH 7) for
384 15 min at room temperature, dehydrated by passing through a gradient of ice-cold methanol (50%, 75%,
385 100%) for 3 minutes each, then sealed and stored at 4°. The next day, the GOCs were rehydrated using
386 the reverse methanol gradient (75%, 50%, PBS) for 3 minutes each. Up to 10 GOCs were placed in the
387 middle of a glass microscope slide, encircled by a hydrophobic barrier created using an Immedge pen, and
388 incubated with protease solution (ACD, 322337) for 20 min. Slides were rinsed 3 times with PBS and
389 processed as indicated by the manufacturer for the BaseScope Assay (Advanced Cell Diagnostics (ACD),
390 323971). Briefly, slides were incubated with the *Smad4* probe specific for the exon8 allele (ACD, 857571)

391 or negative control probe against *Bacillus subtilis DapB* (ACD, 310043) at 40◦C for 2 h in a HybEZ oven.
392 Subsequent amplification and detection steps were performed as recommended by the manufacturer and
393 slides were taken for image acquisition using a Zeiss LSM 880 confocal microscope.

394 **Fluorescence-activated cell sorting**

395 GOCs were dissected from the ovaries of 12-15 d-old *Amhr2-Cre*$^{+}$*; mTmG*$^{+}$*; Smad4*$^{fl/fl}$ mice or were
396 collected after tamoxifen treatment and culture in the case of *ER-Cre+; mTmG+ Smad4*$^{fl/fl}$ mice. GOCs
397 were dissected from *Amhr2-Cre*$^{-}$ and *ER-Cre-* littermates were used as negative controls of EGFP
398 expression**.** They were transferred to a 4-well dish containing Ca-free MEM (Thermo Fisher, 21068028)
399 supplement with 0.25% trypsin (Thermo Fisher, 25200056), 1mM EDTA (Sigma) and DNAse I for several
400 minutes. After pipetting up and down for a few times to dissociate the cells, fetal bovine serum was added
401 (4% final concentration) to inactivate the trypsin. Cells were centrifuged at 1500xg for 5 minutes and
402 supernatant was carefully removed under the dissecting microscope to better visualise the pellet. FACs
403 buffer containing PBS, 1%FBS, 1mM EDTA and 1mg/ml of DAPI was used to resuspend the pellet. Cells
404 were resuspended and passed through a Flowmi® 40-µm strainer (Merck,BAH136800040) to remove
405 oocytes and cell clumps, and then kept on ice for sorting. Resulting granulosa cells were analyzed on a BD
406 FACSAria Fusion 8.0.2 sorter at the Immunophenotyping Facility of the RI-MUHC. All events were collected
407 for each sample. A 488-nm excitation laser was used for both Tomato and EGFP excitation since the
408 wavelength of 488 nm falls within the peak excitation of EGFP but only at 25% of peak excitation for
409 tdTomato. Data were analyzed using FlowJo FACS analysis software. Cells were gated for singlets (using
410 forward scatter vs. side scatter area), viability (DAPI scatter vs. side scatter area)], and fluorescence (FITC
411 and PE) without compensation.

412 **Measurement of granulosa cell-oocyte communication using fluorescence recovery after**
413 **photobleaching (FRAP)**

414 A protocol for FRAP was adapted from our previous study (El-Hayek & Clarke, 2015). GOCs were incubated
415 for 15 min in MEM supplemented with calcein-AM and then for 60 min in calcein-free MEM to allow
416 transfer of calcein from the granulosa cells into oocyte. A circular region of interest of fixed diameter (10
417 µm, to ensure the bleaching did not extend to the surrounding granulosa cells) was set in the center of
418 the enclosed oocyte and subjected to 60 repetitive bleaches of 50 iterations (1 min total duration) using
419 the argon laser at 50% transmission strength. The intensity of fluorescence in the oocyte and the layer of
420 granulosa cells immediately surrounding it was recorded before bleaching and after the 10th, 20th, 30th,
421 40th, 50th, and 60th bleaching. Fluorescence was calculated as intensity of fluorescence in granulosa cell
422 layer at each time point divided by the pre-bleach intensity of the layer. As oocytes of all experimental
423 groups were subjected to the same bleaching procedure within the fixed ROI, the loss in fluorescence was
424 further divided by initial pre-bleach intensity of the oocyte normalized to intensity of fluorescence in
425 oocyte at the given time point, in order to correct for differences in bleaching effect in oocytes of different
426 sizes.

427 **Generation of granulosa cell-oocyte reaggregates**

428 GOCs were obtained from 12-day *ER/Cre*$^{+}$*; mTmG*$^{+}$*; Smad4*$^{+/+}$ and *ER-Cre*$^{+}$*; mTmG*$^{+}$*; Smad4*$^{fl/fl}$ mice,
429 exposed to tamoxifen for 24 hr and incubated for an additional five days as described above. They were
430 then incubated in Ca-Mg-free PBS and drawn in and out of a mouth-controlled micropipette to generate
431 a suspension of denuded oocytes surrounded by the zona pellucida and individual or small clumps of
432 granulosa cells. Briefly, the granulosa cells were deposited together with oocytes from CD-1 mice into the
433 base of a 200-µl microfuge tube and PBS was added to a total volume of 100 µl. The tube was spun at top
434 speed in a microcentrifuge for one minute, then rotated 180° and centrifuged for one minute. This step
435 was repeated twice more. The tube was then cut near the base and the cell-pellet was carefully scooped
436 out and incubated for 2 days in 4-well plates in MEM supplemented with FSH, estradiol and ITS. At the

437 end of the incubation period, complexes of oocytes surrounded by granulosa cells were fixed and
438 processed for analysis.

439 **Image analysis**

440 To quantify the number of F-actin-stained-TZPs, a confocal optical section was obtained at the equatorial
441 plane of the oocyte. Using Fiji software (National Institutes of Health, Bethesda, MD), a segmented circle
442 was drawn around the oocyte in the middle of the zona pellucida, and the fluorescence intensity at each
443 point on the line was obtained. Each point whose value was above the background value of the oocyte
444 cytoplasm and higher than each of its immediately neighboring points was counted as a TZP.

445 To quantify EdU incorporation in granulosa cells, Fiji was used to calculate the ratio of Edu-labelled cells
446 per GOC by dividing the number of EdU-positive cells by the total number of cells counterstained with
447 DAPI.

448 To individually segment granulosa cells and their corresponding TZPs, Imaris 9.7.2 Software (Bitplane) was
449 used. First, z-stacks of 0.2 µm thickness covering the middle region of a follicle were imaged to obtain a
450 conventional 2D Maximum Intensity Projection (MIP). Then, a 3D rendered segmentation of GFP-positive
451 granulosa cells was created with the "Cell detection" tool where cell boundaries were detected based on
452 GFP membrane staining. Smallest diameter was set to 100µm, membrane detail of 0.2 µm and the
453 threshold was adjusted based on local contrast. Segmented cells with a volume less than 100µm^2 were
454 deleted and fusing or fragmented cells were edited using the "merge" or "split" tools to match the original
455 image. The oocyte was also segmented using the phalloidin red channel. After edition, cells were
456 converted to surface objects with the tool "Convert to surfaces" to record their measurements. To render
457 individual TZPs, the "Filament tracer" tool and semi-automated tracing with the tool "Autopath" was used
458 to draw the path of each TZP from the granulosa cell body (start) to the oocyte surface (end)

459 (Supplemental Figure 1A). TZP diameter (thickness) was calculated automatically with a minimum
460 diameter of 0.1 µm. To determine the distance of the TZP tip to the oocyte surface, the segmented TZP
461 was automatically divided into discrete spots using the extension "Filament to Spots". This allowed the
462 calculation of the distance from each spot to the oocyte surface. All measurements were exported using
463 the "distance to oocyte surface" from each TZP spot. To determine the TZP orientation (away or towards
464 the oocyte), the distance of the spot located at the TZP start was subtracted from the distance of the spot
465 located at the TZP tip. A positive difference indicates that the TZP tip is closer to the oocyte and a negative
466 difference indicates that the TZP tip is farther from the oocyte (Supplemental Figure 1B).

467 **Statistical analysis**

468 Data are presented as mean ± standard error of mean and were analyzed and represented using GraphPad
469 Prism 8.4.2 software. Statistical significance was evaluated using one- or two-sample two-tailed t-tests.

470 **Acknowledgements**

471 We thank Drs. Shibo Feng and Min Fun (RI-MUHC Imaging Platform) and Marie-Hélène Lacombe, Hélène
472 Pagé-Veillette and Dr. Ekaterina Iourtchenko (RI-MUHC Immunophenotyping Platform) for their
473 invaluable assistance. We thank Drs Milan Ešner and Wojciech Jesionek (CELLIM core facility, CEITEC MU,
474 Czechia) for their generous support and assistance in obtaining image analysis data using Imaris, and our
475 colleagues for advice and discussion. Supported by grants to H.J.C. from the Canadian Institutes of Health
476 Research and the Natural Sciences and Engineering Research Council. H.J.C. gratefully acknowledges the
477 support of the Richard Cruess Chair in Reproductive Biology at McGill University.

478 **Author contributions**

479 Conceptualization: S.G.A. and H.C.

480 Methodology: S.G.A., Q.Y. and H.C.

481 Investigation: S.G.A. and Q.Y.

482 Funding acquisition: H.C.

483 Supervision: S.G.A. and H.C.

484 Writing – original draft: S.G.A. and H.C.

485 Writing – review and editing: All authors have read and agreed to the final version of the manuscript.

486 **Conflict of interest**

487 The authors declare no conflicts of interest.

488 **References**

489 Aashaq S, Batool A, Mir SA, Beigh MA, Andrabi KI, Shah ZA (2022) TGF-β signaling: A recap of SMAD-
490 independent and SMAD-dependent pathways. *J Cell Physiol* 237: 59-85

491 Albertini DF, Rider V (1994) Patterns of intercellular connectivity in the mammalian cumulus-oocyte
492 complex. *Microsc Res Techn* 27: 125-133

493 Aragón E, Wang Q, Zou Y, Morgani SM, Ruiz L, Kaczmarska Z, Su J, Torner C, Tian L, Hu J *et al* (2019)
494 Structural basis for distinct roles of SMAD2 and SMAD3 in FOXH1 pioneer-directed TGF-β signaling.
495 *Genes Dev* 33: 1506-1524

496 Baena V, Terasaki M (2019) Three-dimensional organization of transzonal projections and other
497 cytoplasmic extensions in the mouse ovarian follicle. *Sci Rep* 9: 1262

498 Carabatsos MJ, Elvin J, Matzuk MM, Albertini DF (1998) Characterization of oocyte and follicle
499 development in growth differentiation factor-9-deficient mice. *Dev Biol* 204: 373-384

500 Carabatsos MJ, Sellitto C, Goodenough DA, Albertini DF (2000) Oocyte-granulosa cell heterologous gap
501 junctions are required for the coordination of nuclear and cytoplasmic meiotic competence. *Dev Biol*
502 226: 167-179

503 Clarke HJ (2018) Regulation of germ cell development by intercellular signaling in the mammalian
504 ovarian follicle. *Wiley Interdiscip Rev Dev Biol* 7: 10.1002/wdev.1294

505 Clarke HJ (2022) Transzonal projections: Essential structures mediating intercellular communication in
506 the mammalian ovarian follicle. *Mol Reprod Dev* 89: 509-525

507 Crozet F, Letort G, Bulteau R, Da Silva C, Eichmuller A, Tortorelli AF, Blévinal J, Belle M, Dumont J, Piolot
508 T *et al* (2023) Filopodia-like protrusions of adjacent somatic cells shape the developmental potential of
509 oocytes. *Life Sci Alliance* 6

510 Derynck R, Budi EH (2019) Specificity, versatility, and control of TGF-β family signaling. *Sci Signal* 12

511 Doherty CA, Amargant F, Shvartsman SY, Duncan FE, Gavis ER (2022) Bidirectional communication in
512 oogenesis: a dynamic conversation in mice and Drosophila. *Trends Cell Biol* 32: 311-323

513 Dong J, Albertini DF, Nishimori K, Kumar RM, Lu N, Matzuk M (1996) Growth differentiation factor-9 is
514 required during early ovarian folliculogenesis. *Nature* 383: 531-535

515 Dragovic RA, Ritter LJ, Schulz SJ, Amato F, Thompson JG, Armstrong DT, Gilchrist RB (2007) Oocyte-
516 secreted factor activation of SMAD 2/3 signaling enables initiation of mouse cumulus cell expansion. *Biol*
517 *Reprod* 76: 848-857

518 El-Hayek S, Clarke HJ (2016) Control of oocyte growth and development by intercellular communication
519 within the follicular niche. *Res Probl Cell Differ* 58: 191-224

520 El-Hayek S, Yang Q, Abbassi L, FitzHarris G, Clarke HJ (2018a) Mammalian oocytes locally remodel
521 follicular architecture to provide the foundation for germline-soma communication. *Curr Biol* 28: 1124-
522 1131

523 El-Hayek S, Yang Q, Clarke HJ (2018b) Growth in vitro of granulosa cell-oocyte complexes of the mouse.
524 *Methods Mol Biol* 1818: 1-11

525 Elvin J, Yan C, Wang P, Nishimori K, Matzuk M (1999a) Molecular characterization of the follicular
526 defects in the growth differentiation factor 9-deficient ovary. *Mol Endocrinol* 13: 1018 - 1034

527 Elvin JA, Clark AT, Wang P, Wolfman NM, Matzuk MM (1999b) Paracrine actions of growth
528 differentiation factor-9 in the mammalian ovary. *Mol Endocrinol* 13: 1035-1048

529 Eppig JJ (1979) A comparison between oocyte growth in coculture with granulosa cells and oocytes with
530 granulosa cell-oocyte junctional contact maintained in vitro. *J Exp Zool* 209: 345-353

531 Fierro-Gonzalez JC, White MD, Silva JC, Plachta N (2013) Cadherin-dependent filopodia control
532 preimplantation embryo compaction. *Nat Cell Biol* 15: 1424-1433

533 Gallop JL (2020) Filopodia and their links with membrane traffic and cell adhesion. *Semin Cell Dev Biol*
534 102: 81-89

535 Gittens JE, Kidder GM (2005) Differential contributions of connexin37 and connexin43 to oogenesis
536 revealed in chimeric reaggregated mouse ovaries. *J Cell Sci* 118: 5071-5078

537 Granados-Aparici S, Hardy K, Franks S, Sharum IB, Waite SL, Fenwick MA (2019) SMAD3 directly
538 regulates cell cycle genes to maintain arrest in granulosa cells of mouse primordial follicles. *Sci Rep* 9:
539 6513

540 Guglielmi L, Heliot C, Kumar S, Alexandrov Y, Gori I, Papaleonidopoulou F, Barrington C, East P,
541 Economou AD, French PMW *et al* (2021) Smad4 controls signaling robustness and morphogenesis by
542 differentially contributing to the Nodal and BMP pathways. *Nature communications* 12: 6374

543 Hao X, Yuan F, Cui Y, Zhang M (2022) Oocyte-secreted factor TGFB2 enables mouse cumulus cell
544 expansion in vitro. *Mol Reprod Dev* 89: 554-562

545 Hardy K, Mora JM, Dunlop C, Carzaniga R, Franks S, Fenwick MA (2018) Nuclear exclusion of SMAD2/3 in
546 granulosa cells is associated with primordial follicle activation in the mouse ovary. *J Cell Sci* 131

547 Heckman CA, Plummer HK, 3rd (2013) Filopodia as sensors. *Cell Signal* 25: 2298-2311

548 Herta A-C, Akin N, Billooye K, Saucedo-Cuevas L, Lolicato F, Segers I, Anckaert E, Smitz J (2021) Reversing
549 complete mechanical transzonal projections disruption during mouse in vitro follicle culture with
550 unaltered oocyte competence†. *Biol Reprod* 104: 1373-1385

551 Jaffe LA, Egbert JR (2016) Regulation of mammalian oocyte meiosis by intercellular communication
552 within the ovarian follicle. *Ann Rev Physiol* 79: 237-260

553 Jorgensen JS (2013) Defining the neighborhoods that escort the oocyte through its early life events and
554 into a functional follicle. *Mol Reprod Dev* 80: 960-976

555 Jorgez CJ, Klysik M, Jamin SP, Behringer RR, Matzuk MM (2004) Granulosa Cell-Specific Inactivation of
556 Follistatin Causes Female Fertility Defects. *Mol Endocrinol* 18: 953-967

557 Kang Y, Ling J, Suzuki R, Roife D, Chopin-Laly X, Truty MJ, Chatterjee D, Wang H, Thomas RM, Katz MH *et*
558 *al* (2014) SMAD4 regulates cell motility through transcription of N-cadherin in human pancreatic ductal
559 epithelium. *PLoS One* 9: e107948

560 Kessel RG, Tung HN, Roberts R, Beams HW (1985) The presence and distribution of gap junctions in the
561 oocyte-follicle cell complex of the zebrafish, Brachydanio rerio. *J Submicrosc Cytol* 17: 239-253

562 Knight PG, Glister C (2006) TGF-beta superfamily members and ovarian follicle development.
563 *Reproduction* 132: 191-206

564 Li R, Albertini DF (2013) The road to maturation: somatic cell interaction and self-organization of the
565 mammalian oocyte. *Nat Rev Mol Cell Biol* 14: 141-152

566 Li Y, Schang G, Wang Y, Zhou X, Levasseur A, Boyer A, Deng CX, Treier M, Boehm U, Boerboom D *et al*
567 (2018) Conditional Deletion of FOXL2 and SMAD4 in Gonadotropes of Adult Mice Causes Isolated FSH
568 Deficiency. *Endocrinology* 159: 2641-2655

569 Litscher ES, Wassarman PM (2020) Zona pellucida proteins, fibrils, and matrix. *Annu Rev Biochem* 89:
570 695-715

571 Macaulay AD, Gilbert I, Caballero J, Barreto R, Fournier E, Tossou P, Sirard MA, Clarke HJ, Khandjian EW,
572 Richard FJ *et al* (2014) The gametic synapse: RNA transfer to the bovine oocyte. *Biol Reprod* 91: 90

573 Marchais M, Gilbert I, Bastien A, Macaulay A, Robert C (2022) Mammalian cumulus-oocyte complex
574 communication: a dialog through long and short distance messaging. *J Assist Reprod Genet*

575 Mattila PK, Lappalainen P (2008) Filopodia: molecular architecture and cellular functions. *Nat Rev Mol*
576 *Cell Biol* 9: 446-454

577 McGinnis LK, Kinsey WH (2015) Role of focal adhesion kinase in oocyte-follicle communication. *Mol*
578 *Reprod Dev* 82: 90-102

579 Mora JM, Fenwick MA, Castle L, Baithun M, Ryder TA, Mobberley M, Carzaniga R, Franks S, Hardy K
580 (2012) Characterization and significance of adhesion and junction-related proteins in mouse ovarian
581 follicles. *Biol Reprod* 86: 153

582 Motta P, Makabe S, Naguro T, Correr S (1994) Oocyte follicle cells association during development of
583 human ovarian follicle. A study by high resolution scanning and transmission electron microscopy. *Arch*
584 *Histol Cytol* 57: 369 - 394

585 Mottershead DG, Sugimura S, Al-Musawi SL, Li JJ, Richani D, White MA, Martin GA, Trotta AP, Ritter LJ,
586 Shi J *et al* (2015) Cumulin, an oocyte-secreted heterodimer of the transforming growth factor-beta

587 family, is a potent activator of granulosa cells and improves oocyte quality. *J Biol Chem* 290: 24007-
588 24020

589 Nagamatsu G, Shimamoto S, Hamazaki N, Nishimura Y, Hayashi K (2019) Mechanical stress accompanied
590 with nuclear rotation is involved in the dormant state of mouse oocytes. *Sci Adv* 5: eaav9960

591 Norris RP, Ratzan WJ, Freudzon M, Mehlmann LM, Krall J, Movsesian MA, Wang H, Ke H, Nikolaev VO,
592 Jaffe LA (2009) Cyclic GMP from the surrounding somatic cells regulates cyclic AMP and meiosis in the
593 mouse oocyte. *Development* 136: 1869-1878

594 O'Brien MJ, Pendola JK, Eppig JJ (2003) A revised protocol for in vitro development of mouse oocytes
595 from primordial follicles dramatically improves their developmental competence. *Biol Reprod* 68: 1682-
596 1686

597 Pangas SA, Li X, Robertson EJ, Matzuk MM (2006) Premature luteinization and cumulus cell defects in
598 ovarian-specific Smad4 knockout mice. *Mol Endocrinol* 20: 1406-1422

599 Pangas SA, Rajkovic A (2015) Follicular Development: Mouse, Sheep, and Human Models. In: *Knobil and*
600 *Neill's Physiology of Reproduction (Fourth Edition)*, Plant T.M., Zeleznik A.J. (eds.) pp. 947-995. Academic
601 Press: San Diego

602 Patton BK, Madadi S, Pangas SA (2021) Control of ovarian follicle development by TGFβ family signaling.
603 *Curr Opin Endocr Metab Res* 18: 102-110

604 Peng D, Fu M, Wang M, Wei Y, Wei X (2022) Targeting TGF-β signal transduction for fibrosis and cancer
605 therapy. *Mol Cancer* 21: 104

606 Peng J, Li Q, Wigglesworth K, Rangarajan A, Kattamuri C, Peterson RT, Eppig JJ, Thompson TB, Matzuk
607 MM (2013) Growth differentiation factor 9:bone morphogenetic protein 15 heterodimers are potent
608 regulators of ovarian functions. *Proc Natl Acad Sci U S A* 110: E776-785

609 Richani D, Dunning KR, Thompson JG, Gilchrist RB (2021) Metabolic co-dependence of the oocyte and
610 cumulus cells: essential role in determining oocyte developmental competence. *Hum Reprod Update* 27:
611 27-47

612 Robert C (2021) Nurturing the egg: the essential connection between cumulus cells and the oocyte.
613 *Reprod Fertil Dev* 34: 149-159

614 Saatcioglu HD, Cuevas I, Castrillon DH (2016) Control of oocyte reawakening by Kit. *PLoS Genet* 12:
615 e1006215

616 Sagar, Pröls F, Wiegreffe C, Scaal M (2015) Communication between distant epithelial cells by filopodia-
617 like protrusions during embryonic development. *Development* 142: 665-671

618 Schroeder TE (1981) Microfilament-mediated surface change in starfish oocytes in response to 1-
619 methyladenine: implications for identifying the pathway and receptor sites for maturation-inducing
620 hormones. *J Cell Biol* 90: 362-371

621 Simon A, Goodenough D, Li E, Paul D (1997) Female infertility in mice lacking connexin 37. *Nature* 385:
622 525-529

623 Wang ZP, Mu XY, Guo M, Wang YJ, Teng Z, Mao GP, Niu WB, Feng LZ, Zhao LH, Xia GL (2014)
624 Transforming growth factor-beta signaling participates in the maintenance of the primordial follicle pool
625 in the mouse ovary. *J Biol Chem* 289: 8299-8311

626 Wassarman PM, Litscher ES (2018) The mouse egg's zona pellucida. *Curr Top Dev Biol* 130: 331-356

627 Wigglesworth K, Lee KB, O'Brien MJ, Peng J, Matzuk MM, Eppig JJ (2013) Bidirectional communication
628 between oocytes and ovarian follicular somatic cells is required for meiotic arrest of mammalian
629 oocytes. *Proc Natl Acad Sci U S A* 110: E3723-3729

630 Winterhager E, Kidder GM (2015) Gap junction connexins in female reproductive organs: implications for
631 women's reproductive health. *Hum Reprod Update* 21: 340-352

632 Wu X, Chen L, Brown CA, Yan C, Matzuk MM (2004) Interrelationship of growth differentiation factor 9
633 and inhibin in early folliculogenesis and ovarian tumorigenesis in mice. *Mol Endocrinol* 18: 1509-1519

634 Xie J, Xu X, Liu S (2023) Intercellular communication in the cumulus–oocyte complex during
635 folliculogenesis: A review. *Frontiers in Cell and Developmental Biology* 11

636 Yan C, Wang P, DeMayo J, DeMayo FJ, Elvin JA, Carino C, Prasad SV, Skinner SS, Dunbar BS, Dube JL *et al*
637 (2001) Synergistic roles of bone morphogenetic protein 15 and growth differentiation factor 9 in ovarian
638 function. *Mol Endocrinol* 15: 854-866

639 Yang H, Wang L, Zhao J, Chen Y, Lei Z, Liu X, Xia W, Guo L, Zhang HT (2015) TGF-β-activated SMAD3/4
640 complex transcriptionally upregulates N-cadherin expression in non-small cell lung cancer. *Lung Cancer*
641 87: 249-257

642 Yu C, Zhang YL, Fan HY (2013) Selective Smad4 knockout in ovarian preovulatory follicles results in
643 multiple defects in ovulation. *Mol Endocrinol* 27: 966-978

644 Zhang H, Risal S, Gorre N, Busayavalasa K, Li X, Shen Y, Bosbach B, Brännström M, Liu K (2014) Somatic
645 cells initiate primordial follicle activation and govern the development of dormant oocytes in mice. *Curr*
646 *Biol* 24: 2501-2508

647 Zhang M, Su YQ, Sugiura K, Xia G, Eppig JJ (2010) Granulosa cell ligand NPPC and its receptor NPR2
648 maintain meiotic arrest in mouse oocytes. *Science* 330: 366-369

649 Zhang Y, Wang Y, Feng X, Zhang S, Xu X, Li L, Niu S, Bo Y, Wang C, Li Z *et al* (2021) Oocyte-derived
650 microvilli control female fertility by optimizing ovarian follicle selection in mice. *Nature communications*
651 12: 2523

652

653

Figure 1

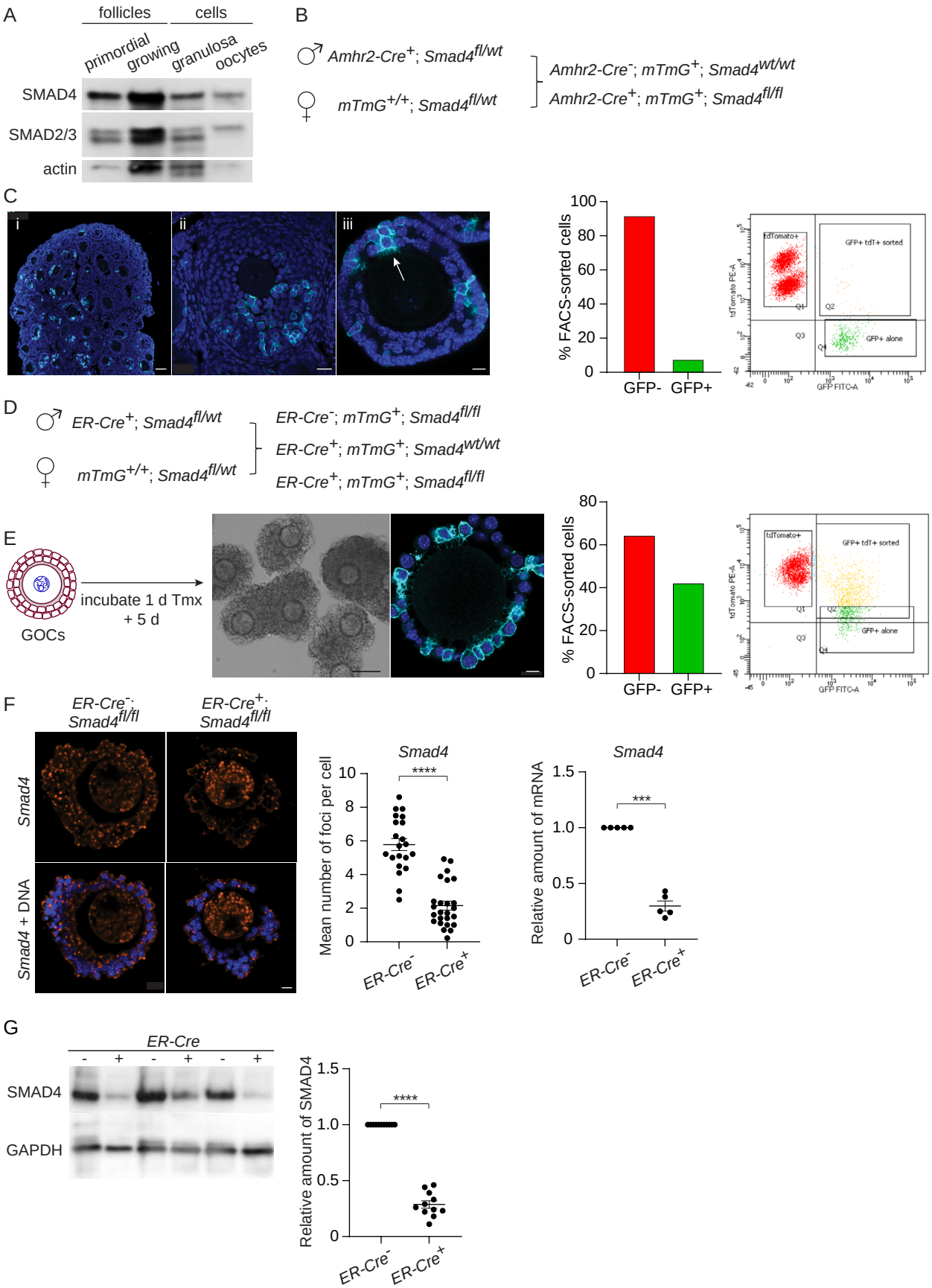
A
follicles
cells
primordial
growing
granulosa
oocytes
SMAD4
SMAD2/3
actin
B
♂ Amhr2-Cre+; Smad4fl/wt
♀ mTmG+/+; Smad4fl/wt
Amhr2-Cre-; mTmG+; Smad4wt/wt
Amhr2-Cre+; mTmG+; Smad4fl/fl
C
i
ii
iii
% FACS-sorted cells
GFP-
GFP+
tdTomato+
GFP+ tdT+ sorted
GFP+ alone
tdTomato PE-A
GFP FITC-A
D
♂ ER-Cre+; Smad4fl/wt
♀ mTmG+/+; Smad4fl/wt
ER-Cre-; mTmG+; Smad4fl/fl
ER-Cre+; mTmG+; Smad4wt/wt
ER-Cre+; mTmG+; Smad4fl/fl
E
GOCs
incubate 1 d Tmx
+ 5 d
% FACS-sorted cells
GFP-
GFP+
F
ER-Cre-; Smad4fl/fl
ER-Cre+; Smad4fl/fl
Smad4
Smad4 + DNA
Smad4
Mean number of foci per cell
****
ER-Cre-
ER-Cre+
Smad4
Relative amount of mRNA
***
ER-Cre-
ER-Cre+
G
ER-Cre
SMAD4
GAPDH
Relative amount of SMAD4
****
ER-Cre-
ER-Cre+

655 **Figure 1. SMAD4 is efficiently depleted in granulosa cells of GOCs in vitro using tamoxifen-induced Cre**
656 **recombinase**

657 A. Immunoblot of primordial follicles, growing follicles, and granulosa cells and oocytes isolated from
658 antral follicles, probed using anti-SMAD4 and anti-SMAD2/3.
659 B. Breeding scheme to delete *Smad4* in the granulosa cells using *Amhr2-Cre*. The *mTmG* cassette
660 enables Cre recombinase activity to be verified through expression of EGFP.
661 C. Left: Confocal images of histological sections of paraffin-embedded 12-d ovary (i, ii) and an isolated
662 follicle (iii) stained using an anti-GFP antibody and DAPI to counterstain DNA. Relatively few
663 granulosa cells are GFP-positive (arrow in iii). Scale bars: 50 µm, 20 µm, 10 µm. Right: Histogram and
664 chart showing the percentage of FACS-sorted GFP+ and GFP- granulosa cells from growing follicles.
665 Granulosa cells expressing both td tomato and GFP and GFP alone were scored as GFP+.
666 D. Breeding scheme to delete *Smad4* in vitro using generate tamoxifen-inducible *ER-Cre*. The *mTmG*
667 cassette enables Cre recombinase activity to be verified through expression of EGFP.
668 E. Left: Schematic illustrating time-line of GOC exposure to tamoxifen and subsequent incubation.
669 Center: Bright-field image of GOCs following incubation and confocal image of a representative GOC
670 stained using anti-GFP antibody and DAPI to counterstain DNA. Scale bar = 10µm and 100µm,
671 respectively. Right: Bar chart showing the percentage of FACS-sorted GFP+ and GFP- granulosa cells
672 from GOCs. Granulosa cells expressing td tomato and GFP and GFP alone are counted as GFP+.
673 F. Left: Confocal image of representative GOCs stained with single-molecule RNA FISH probe for *Smad4*
674 exon 8 and DAPI to counterstain DNA. Right: Mean and SEM of the average number of *Smad4* mRNA
675 foci per cell (left) and relative mRNA amounts of *Smad4* quantified using qRT-PCR (right) in granulosa
676 cells five days after tamoxifen treatment.
677 G. Immunoblot and plot of mean and SEM of SMAD4 protein content in granulosa cells from GOCs five
678 days after tamoxifen treatment.

679 Statistical analysis using t-test (F, left) and one-sample t-test (F, right and G), ***P< 0.001; ****P <

680 0.0001.

681

Figure 2

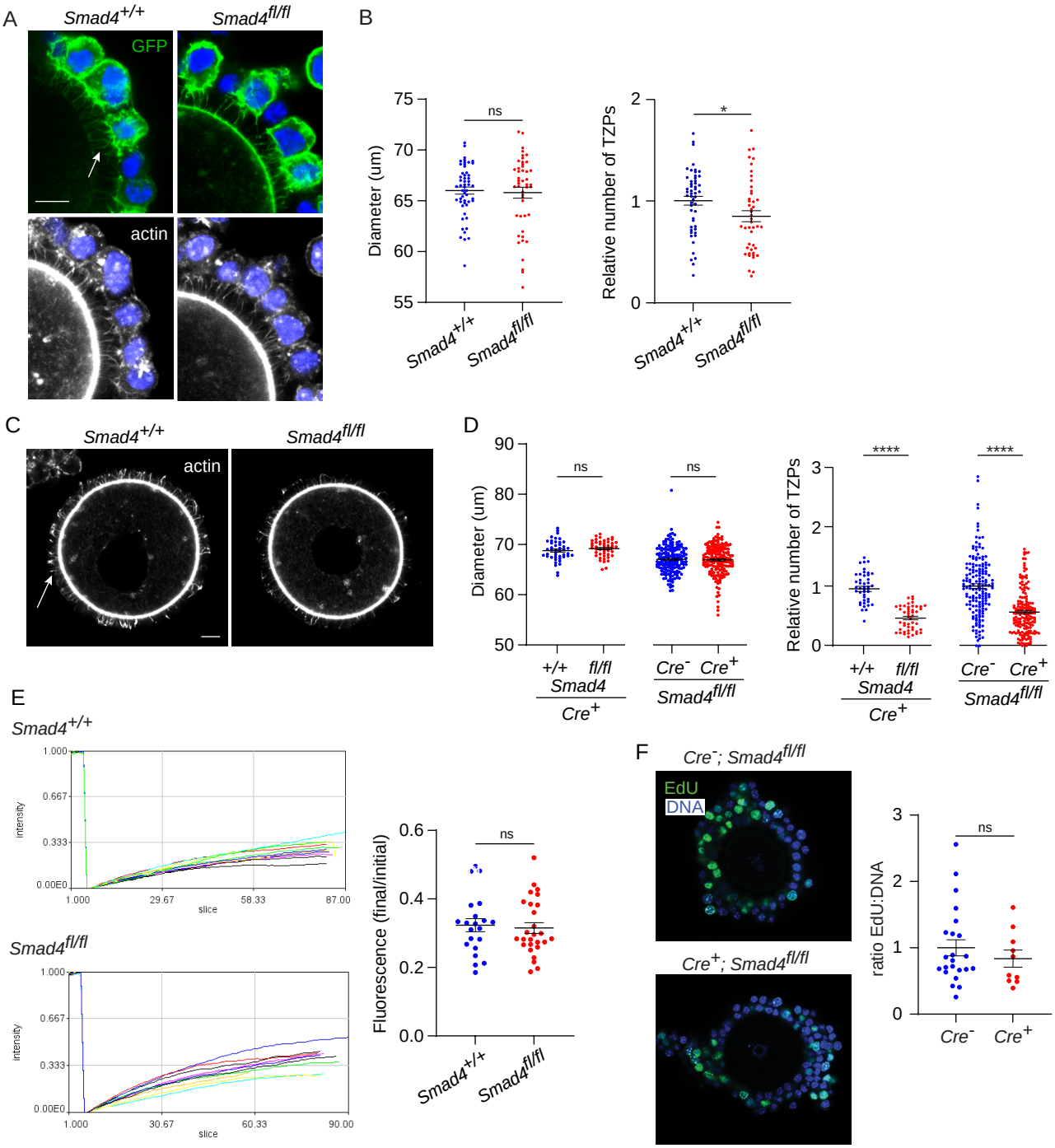
A
Smad4+/+
Smad4fl/fl
GFP
actin
B
Diameter (um)
ns
Relative number of TZPs
*
Smad4+/+
Smad4fl/fl
C
Smad4+/+
Smad4fl/fl
actin
D
Diameter (um)
ns
ns
Relative number of TZPs
****
****
+/+
fl/fl
Smad4
Cre+
Cre-
Cre+
Smad4fl/fl
E
Smad4+/+
intensity
slice
Smad4fl/fl
intensity
slice
Fluorescence (final/initial)
ns
Smad4+/+
Smad4fl/fl
F
Cre-; Smad4fl/fl
EdU
DNA
Cre+; Smad4fl/fl
ratio EdU:DNA
ns
Cre-
Cre+

683 **Figure 2. Depletion of SMAD4 reduces TZP-number but does not affect granulosa cell communication**
684 **with the oocyte or proliferation.**

685 A. Confocal images of GOCs five days after tamoxifen treatment stained with anti-GFP, phalloidin to
686 visualize F-actin and DAPI to counterstain DNA. Arrow shows GFP-labelled TZPs. Scale bar = 20 µm.

687 B. Mean and SEM of oocyte diameter and TZP number five days after tamoxifen treatment. TZP
688 number in each GOC is normalized to the oocyte diameter.

689 C. Confocal image of a denuded GOC five days after tamoxifen treatment and removal of the
690 granulosa cells, stained with anti-GFP, phalloidin to visualize F-actin and DAPI to counterstain DNA.
691 Arrow shows phalloidin-labelled TZPs that remain embedded in the zona pellucida. Scale bar =
692 20µm.

693 D. Mean and SEM of oocyte diameter and TZP number five days after tamoxifen treatment in denuded
694 GOCs. TZP number for each specimen is normalized to the oocyte diameter.

695 E. Left: Time course of fluorescence recovery in oocyte of GOCs following bleaching. Each line
696 represents an individual GOC. Right: Mean and SEM of the ratio of the final to pre-bleach
697 fluorescence in each GOC.

698 F. Left: Confocal image of a GOC after tamoxifen treatment followed by treatment with EdU and
699 visualization. DNA stained using DAPI. Scale bar = 20 µm. Right: Mean and SEM of the ratio of Edu-
700 labelled cells to the total number of cells.

701 Statistical analysis using t-test, *P< 0.05; ****P < 0.0001; ns, not significant.

702

Figure 3

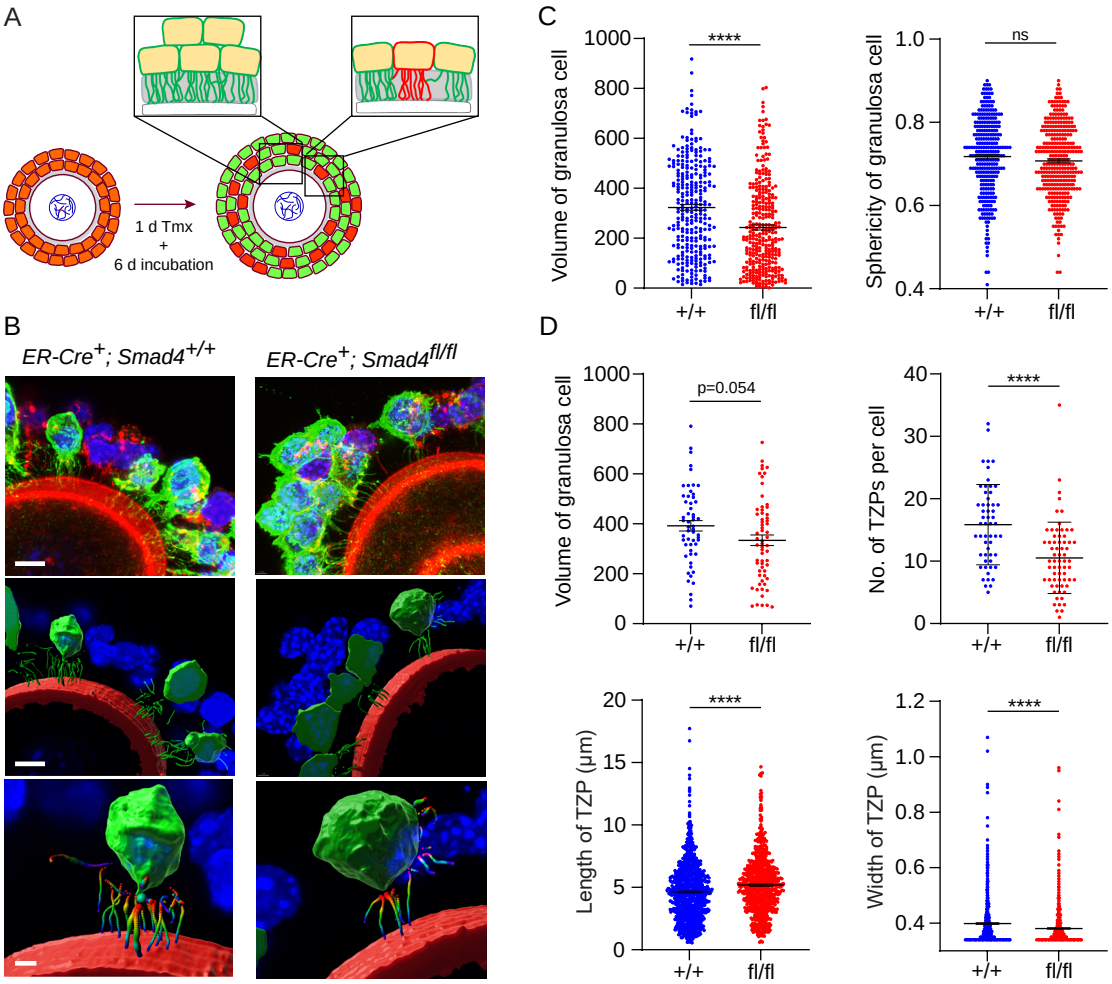
A
1 d Tmx
+
6 d incubation
B
ER-Cre+; Smad4+/+
ER-Cre+; Smad4fl/fl
C
Volume of granulosa cell
****
+/+
fl/fl
Sphericity of granulosa cell
ns
D
Volume of granulosa cell
p=0.054
No. of TZPs per cell
****
Length of TZP (µm)
Width of TZP (µm)

704 **Figure 3. Depletion of SMAD4 in GOCs reduces the number of TZPs per granulosa cell and alters their**

705 **morphometric parameters.**

706 A. Schematic illustrating the experimental protocol. GFP+ granulosa cells in clusters were used for

707 calculations in C and individual GFP+ granulosa cells were used for calculations in D.

708 B. Three-dimensional reconstruction of a GOC, showing granulosa cell bodies, TZPs and oocyte cortex.

709 Serial optical confocal sections were processed using Imaris software. GOCs were stained using

710 anti-GFP (green), phalloidin (red) and DAPI (blue). Scale bar = 10 µm (upper, middle), 3 µm (lower).

711 C. Mean and SEM of volumes and sphericities of individual granulosa cells from a cluster and those

712 selected for TZP analyses.

713 D. Mean and SEM of volumes of individual granulosa cells selected for TZP analysis, number of TZPs

714 per cell, TZP length and width.

715 Statistical analysis using t-test, ****$P < 0.0001$; ns, non-significant.

716

Figure 4

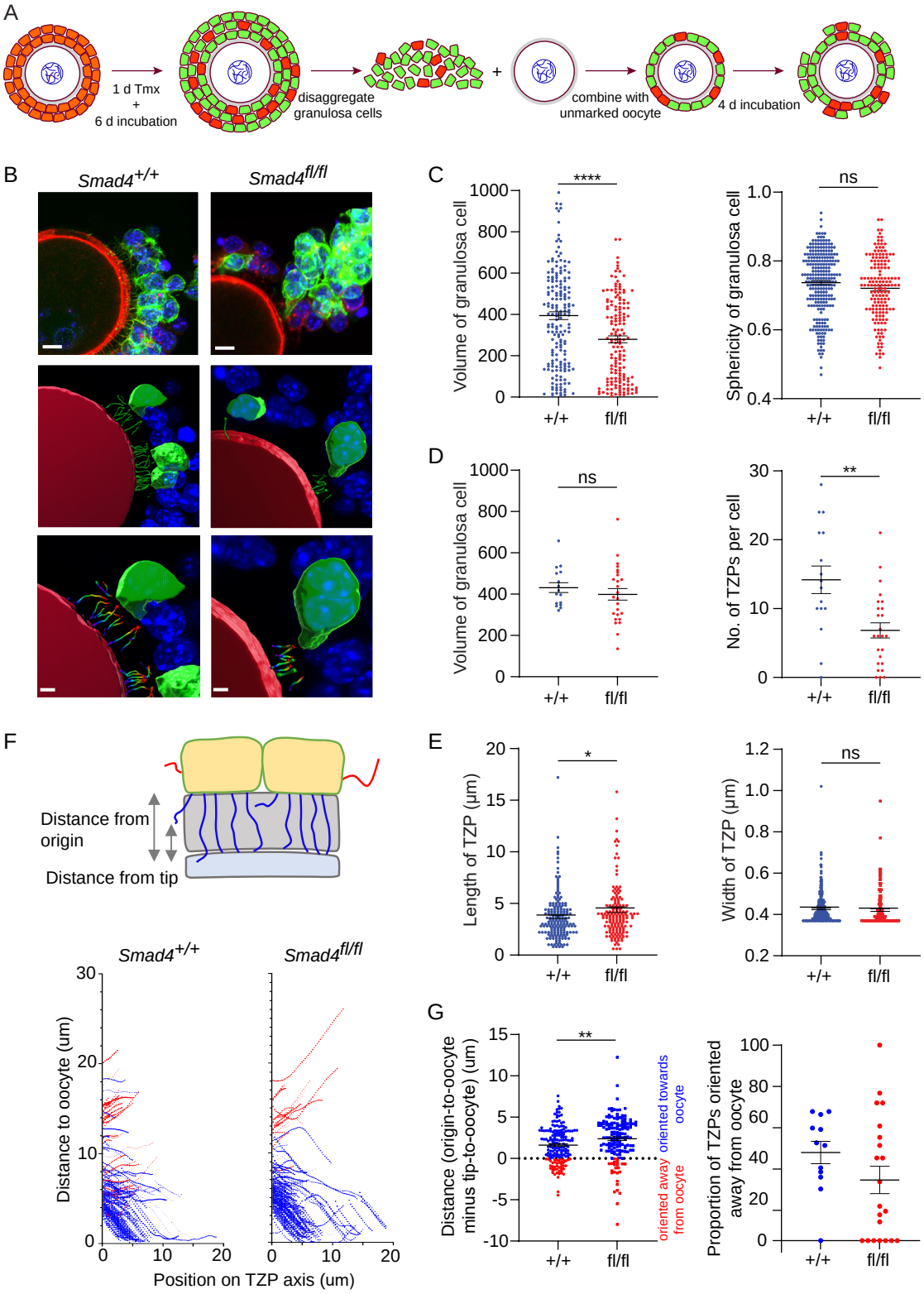
A
1 d Tmx
+
6 d incubation
disaggregate
granulosa cells
+
combine with
unmarked oocyte
4 d incubation
B
Smad4+/+
Smad4fl/fl
C
Volume of granulosa cell
****
Sphericity of granulosa cell
ns
+/+
fl/fl
D
Volume of granulosa cell
ns
No. of TZPs per cell
**
E
Length of TZP (µm)
*
Width of TZP (µm)
ns
F
Distance from
origin
Distance from tip
Smad4+/+
Smad4fl/fl
Distance to oocyte (um)
Position on TZP axis (um)
G
Distance (origin-to-oocyte
minus tip-to-oocyte) (um)
**
oriented towards
oocyte
oriented away
from oocyte
Proportion of TZPs oriented
away from oocyte

718 **Figure 4. Depletion of SMAD4 in reaggregates reduces the number of newly generated TZPs and alters**

719 **their morphometric parameters.**

720 A. Schematic illustrating the reaggregation procedure.

721 B. Three-dimensional reconstruction of a reaggregate, showing granulosa cell bodies, TZPs and oocyte

722 cortex. Serial optical confocal sections were processed using Imaris software. GOCs were stained

723 using anti-GFP (green), phalloidin (red) and DAPI (blue). Scale bar =10 µm (upper), 3 µm (lower).

724 C. Mean and SEM of volumes and sphericities of individual granulosa cells.

725 D, E Mean and SEM of volumes of individual granulosa cells, number of TZPs per cell, TZP length and TZP

726 width.

727 F. Upper: Schematic illustrating how the distance from the origin and the tip, respectively, of TZPs

728 (blue) and non-TZP projections (red) to the oocyte surface was determined. Lower: TZP trajectories

729 of 3D-reconstructed TZPs, representing the distance from origin relative to the position on the TZP

730 axis.

731 G. Left: Mean and SEM of the difference between the distance from the origin and the tip of individual

732 TZPs to the oocyte surface. Blue symbols (>0) represent TZPs oriented towards the oocyte; red

733 symbols (<0) represent non-TZPs oriented away from the oocyte. Right: Mean and SEM of the

734 proportion of TZPs in individual cells that were oriented away from the oocyte.

735 Statistical analysis using t-test, *P < 0.05; **P < 0.01; ****P < 0.0001; ns, non-significant.

736

Figure 5

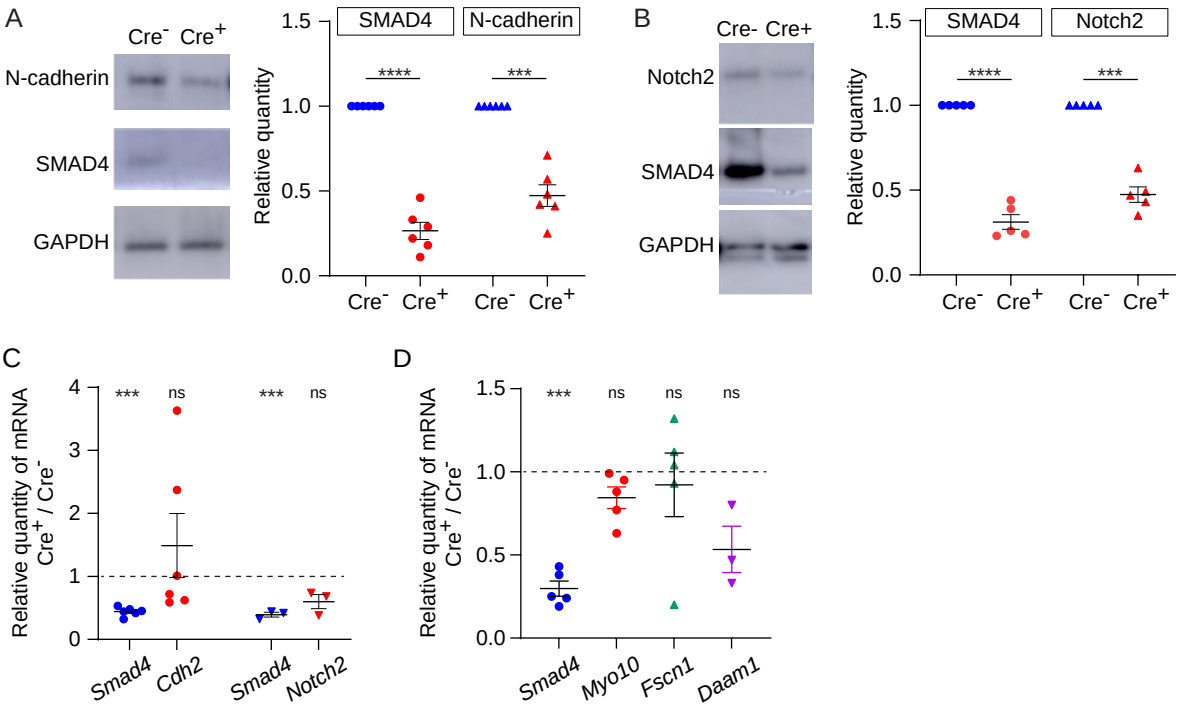
A
Cre- Cre+
N-cadherin
SMAD4
GAPDH
SMAD4
N-cadherin
Relative quantity
1.5
1.0
0.5
0.0
****
***
Cre- Cre+ Cre- Cre+
B
Cre- Cre+
Notch2
SMAD4
GAPDH
SMAD4
Notch2
Relative quantity
1.5
1.0
0.5
0.0
****
***
Cre- Cre+ Cre- Cre+
C
Relative quantity of mRNA Cre+ / Cre-
4
3
2
1
0
***
ns
***
ns
Smad4
Cdh2
Smad4
Notch2
D
Relative quantity of mRNA Cre+ / Cre-
1.5
1.0
0.5
0.0
***
ns
ns
ns
Smad4
Myo10
Fscn1
Daam1

739 **Figure 5. Expression of transmembrane N-cadherin and Notch proteins is reduced in SMAD4-depleted**

740 **granulosa cells.**

741 A. Immunoblot and graph showing mean and SEM of SMAD4 and N-cadherin in granulosa cells.

742 Protein quantities are normalized to amounts in ER-Cre^{-} cells.

743 B. As in A, showing Notch2.

744 C. Mean and SEM of relative mRNA amounts of *Smad4*, *Cdh2* (encoding N-cadherin), and *Notch2* in

745 granulosa cells purified from GOCs five days after tamoxifen treatment. mRNA quantities are

746 normalized to amounts in ER-Cre^{-} cells.

747 D. As in C, showing *Smad4*, *Myo10, Fscn1* and *Daam1*.

748 Statistical analysis using one-sample t-test, ***P < 0.001; ****P < 0.0001; ns non-significant.

749

Figure 6

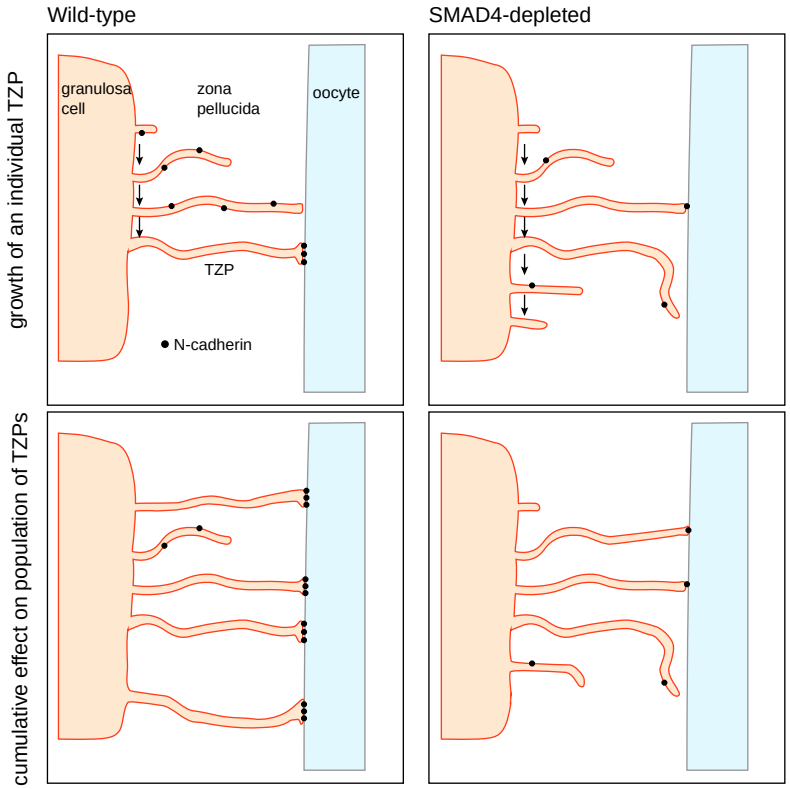
Wild-type
SMAD4-depleted
growth of an individual TZP
cumulative effect on population of TZPs
granulosa cell
zona pellucida
oocyte
TZP
N-cadherin

752 **Figure 6. Model for regulation of the size of the TZP population.**

753 Upper: Dynamics of an individual TZP. When growing TZP contacts the surface of the oocyte, it becomes
754 stably attached if there is sufficient N-cadherin, as in wild-type cells. In SMAD4-depleted cells, there is
755 insufficient N-cadherin to stabilize the attachment. The TZP may continue to elongate but eventually
756 becomes retracted. Lower: Dynamics of the population of TZPs. Owing to increased stability of
757 attachment of individual TZPs to the oocyte surface, the total number of TZPs becomes larger in wild-
758 type cells than in SMAD4-depleted cells.

759

760 **Supplemental Table 1**

761 **Primers, Antibodies, Drugs**

Target	application	5-prime	3-prime	Predicted size
Smad4 -wt	Genotype	GGGCAGCGTAGCATATAAGA	GACCCAAACGTCACCTTCAG	390
Smad4 - flox	Genotype	GGGCAGCGTAGCATATAAGA	GACCCAAACGTCACCTTCAG	450
Smad4 - recombined	Genotype	TAAGAGCCACAGGGTCAAGC	GACCCAAACGTCACCTTCAG	450
Amhr2-Cre	Genotype	CTCTGGTGTAGCTGATGATC	TAATCGCCATCTTCCAGCAG	380
ER-Cre	Genotype	CGTGATCTGCAACTCAGTC	AGGCAAATTTTGGTGTACGG	150
Smad4	mRNA	TCACAATGAGCTTGCATTCC	CCATCCACAGTCACAACAGG	143
Cdh2 (N-Cad)	mRNA	CCAGGAAAAGTGGCAGGTAG	CACTGTGCTTGGCAAGTTGT	121
Notch2	mRNA	GACCCTATCCTACCCTCTAGTG	AGCAGGATGAAGAACAGGATG	103
Myo10	mRNA	TCCAGACAGACTATGGGCAGG	GGAAGCCATGTCGTCCACG	109
Fscn1	mRNA	AGAACGCCAGCTGCTACTTT	CGAGGAATCACTACCCACCG	331
Daam1	mRNA	GCGGCTGCTCAGAGTATAGAAA	AAACATGGCTTCCCTGTGTTTG	273
RPL-19	mRNA	GAAATCGCCAATGCCAACTC	CTTCCCTATGCCCATATGCC	147
RNAScope		**Cat. no. and supplier**		
Smad4	mRNA	857571, Advanced Cell Diagnostics (ACD)		
Antibodies for western		**Cat. no. and supplier**	**Secondary antibody**	
SMAD2/3	protein	8685, Cell Signaling	Goat anti-rabbit IgG-HRP, Promega, W4011	
SMAD4	protein	HPA019154, Sigma	Goat anti-rabbit IgG-HRP, Promega, W4011	
N-cad	protein	B610920, BD Biosciences	Goat anti-mouse IgG-HRP, Promega, W4021	
Notch	protein	ab8926, Abcam	Goat anti-rabbit IgG-HRP, Promega, W4011	
Reagents for IF		**Cat. no. and supplier**	**Secondary antibody**	
GFP	protein	A11122, Invitrogen	Alexa 488 donkey anti-rabbit IgG, A21206, Invitrogen	
Phalloidin	protein	A12380, Thermo Fisher		
Chemicals		**Cat. no. and supplier**		
tamoxifen	Cre activation	T176, Sigma		

EdU	DNA synthesis	C10337, Thermo Fisher		

762

763

764 **Supplemental Figure 1**

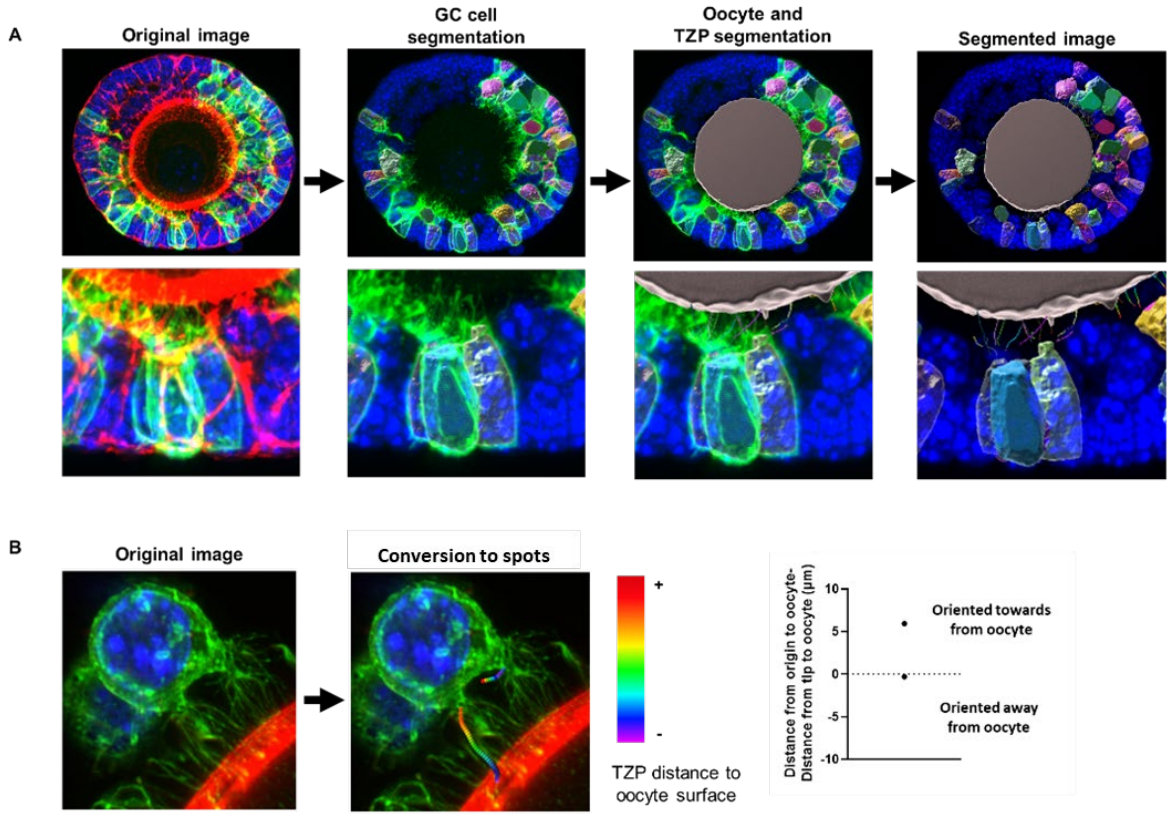

765

766

767

768 **Supplemental Figure 1. Segmentation pipeline of GFP-positive granulosa cells.** (A) 3D reconstruction of granulosa

769 cells, oocyte and TZPs. (B) TZP segmentation into spots. Graph shows an example of spot subtraction of two TZPs

770 oriented towards and away from the oocyte. Heatmap depicts the gradient of colours for the spots that are closer

771 (violet) and farther from the oocyte (red).

772